Anatomical variation of mesophyll conductance due to salt stress in Populus cathayana females and males growing under different inorganic nitrogen sources

Liu, Miao

2021-08

Liu , M , Liu , X , Du , X , Korpelainen , H , Niinemets , U & Li , C 2021 , ' Anatomical variation of mesophyll conductance due to salt stress in Populus cathayana females and males growing under different inorganic nitrogen sources ' , Tree Physiology , vol. 41 , no. 8 , pp. 1462-1478 . https://doi.org/10.1093/treephys/tpab017

http://hdl.handle.net/10138/339732
https://doi.org/10.1093/treephys/tpab017

acceptedVersion

TP-2020-372.R1

Anatomical variation of mesophyll conductance due to salt stress in *Populus cathayana* females and males growing under different inorganic nitrogen sources

Miao Liu [1], Xiucheng Liu [1], Xuhua Du [2],

Helena Korpelainen [3], Ülo Niinemets [4, 5], Chunyang Li [1, *]

[1] College of Life and Environmental Sciences, Hangzhou Normal University, Hangzhou 311121, China

[2] Key Laboratory of State Forestry and Grassland Administration on Bamboo Resources and Utilization, China National Bamboo Research Center, State Forestry and Grassland Administration, Hangzhou 310012, China

[3] Department of Agricultural Sciences, Viikki Plant Science Centre, University of Helsinki, P.O. Box 27, FI-00014, Finland

[4] Institute of Agricultural and Environmental Sciences, Estonian University of Life Sciences, Kreutzwaldi 1, 51006 Tartu, Estonia

[5] Estonian Academy of Sciences, Kohtu 6, 10130 Tallinn, Estonia

* Corresponding author: Chunyang Li, E-mail address: licy@hznu.edu.cn

Running title: Sexually different responses to salt and N forms

Abstract Synergistic regulation in leaf architecture and photosynthesis is essential for salt tolerance. However, how plant sex and inorganic nitrogen sources alter salt stress-dependent photosynthesis remains unknown. Leaf anatomical characteristics and photosynthesis of *Populus cathayana* Rehder females and males were investigated under salt stress conditions combined with NO_3^- and NH_4^+ supplies to clarify the underlying mechanisms. In salt-stressed females, we observed an increased mesophyll spongy cell density, a reduced chloroplast density, a decreased surface area of chloroplasts adjacent to the intercellular air space (S_c/S) and an increased mesophyll cell area per transverse section width (S/W), consequently causing mesophyll conductance (g_m) and photosynthesis inhibition, especially under NH_4^+ supply. Conversely, males with a greater mesophyll palisade tissue thickness and chloroplast density, but a lower spongy cell density had lower S/W and higher S_c/S, and higher g_m and photosynthesis. NH_4^+-fed females had a lower CO_2 conductance through cell wall and stromal conductance perpendicular to the cell wall, but a higher chloroplast conductance from the cell wall (g_{cyt1}) than females supplied with NO_3^-, while males had a higher chloroplast conductance and lower CO_2 conductance through cell wall when supplied with NO_3^- instead of NH_4^+ under salt stress. These findings indicate sex-specific strategies in coping with salt stress related to leaf anatomy and g_m under both types of N supplies, which may contribute to sex-specific CO_2 capture and niche segregation.

Keywords: Leaf anatomy, mesophyll conductance, N form, salt stress, sexual dimorphism

Introduction

Salt stress reduces plant biomass and crop production, and these changes are typically strongly correlated with a decreasing rate of photosynthesis (Praxedes et al. 2010, Wankhade et al. 2013). Photosynthesis is a critical factor that determines energy conversion efficiency, thereby regulating plant productivity and performance (Pinheiro and Chaves 2011, Ort et al. 2015). It has been suggested that CO_2 stomatal limitations, including stomatal (g_s) and mesophyll (g_m) conductance limitation, are primary factors restricting leaf photosynthesis (A) in salt-stressed leaves (Flexas et al. 2016, Zait et al. 2019, Veromann-Jürgenson et al. 2020). Leaf dehydration induced by drought and/or salt stress reduces g_s to control the transpirational water flow from leaves (Golldack et al. 2014). However, lower g_s reduces CO_2 flux into leaves, and then results in the limitation of A and carbon starvation in plants. The g_m value indicates CO_2 diffusion from the sub-stomatal cavities to the sites of carboxylation. According to a previous simulation performed by Zhu et al. (2010), doubling of g_m could improve photosynthetic rates by nearly 20% under normal growth conditions. In stressed plants, the photosynthetic limitation due to g_m can be much greater than in non-stressed plants (Martins et al. 2014, Niinemets and Keenan 2014). Therefore, it is important to clarify, whether and how salt stress affects g_m and then leaf A in dioecious plants.

The g_m values of given genotypes or species are associated with changes in leaf anatomical traits, especially under environmental stresses (Niinemets et al. 2009a, Lu et al. 2016). Generally, leaves with a robust structure and higher *LMA* show lower g_m and photosynthesis (Niinemets et al. 2009b, Tomás et al. 2013). Plants with higher *LMA* usually have a greater biomass investment in supporting tissues, thicker cell walls, a lower cytoplasm and higher stroma conductance to CO_2 diffusion inside leaves (Niinemets 2007, Tomás et al. 2013). Inside a leaf, CO_2 from substomatal cavities diffuses through the intercellular air space and liquid phase consisting of the cell wall, cytoplasm, plasma membrane, chloroplast stroma and envelope (Tosens et al. 2012b, Cano et al. 2013). The CO_2 liquid-phase resistance accounts for 80-90% of mesophyll resistance (Lu et al. 2016, Tosens et al. 2016).

Among CO_2 liquid-phase diffusion components, the cell wall thickness of the leaf mesophyll and the chloroplast surface area exposed to intercellular air space (S_c/S) have been considered as the strongest limiting factors of g_m, but these traits are highly different among species (Tomás et al. 2013, Berghuijs et al. 2016). An increased mesophyll cell wall thickness and decreased S_c/S can probably increase the CO_2 diffusion path length and area, which will limit g_m in plants (Terashima et al. 2011, Tomás et al. 2013). In addition, the increased mesophyll surface area exposed to the intercellular air space (S_m/S) facilitates CO_2 diffusion from the cytosol into chloroplasts, which promotes photosynthesis via greater g_m (Ren et al. 2019, Hu et al.

2020). Other cellular components, such as chloroplasts, plasmalemma and cytoplasm also affect CO_2 diffusion into leaves (Tomás et al. 2013, Lu et al. 2016). A higher mesophyll cell density typically decreases the air space size, which probably decreases the CO_2 gas-phase conductance (Tomás et al. 2013, Lu et al. 2016). Also, a recent study has indicated that a large total mesophyll cell area per transverse section width (S/W) is advantageous as balancing the leaf structure and CO_2 assimilation (Hu et al. 2020). Therefore, knowledge of leaf structural and anatomical traits affecting g_m is crucial for understanding photosynthetic efficiency, especially under abiotic stresses.

Generally, salt stress induces leaf dehydration and leads to the reduction of g_m and g_s in plants (Wang et al. 2018, Zait et al. 2019). Leaf dehydration reduces the internal air space volume and increases the cell wall thickness (Henry et al. 2000, Tosens et al. 2012a). The size and shape of chloroplasts and mesophyll cells are also strongly affected by leaf dehydration (Scoffoni et al. 2017). Such changes probably have major implications for g_m (Tosens et al. 2012a) and suggest that salt stress may lead to analogous changes. How g_m is affected by salinity is still an open question, especially in trees. Moreover, little is known about the effects of salt stress on leaf anatomy and photosynthesis under different inorganic N sources, e.g. NH_4^+ vs. NO_3^-.

Poplars are dioecious species, in which females and males have significant differences in biomass partitioning, photosynthesis, carbon-nutrient balance and leaf anatomical

traits when exposed to abiotic stresses, including salt stress (Li et al. 2016, Chen et al. 2016, Liu et al. 2020a, Liu et al. 2021), which is further affected by N forms (Chen et al. 2011, Liu et al. 2020b). Poplars preferentially take up NO_3^- when both NH_4^+ and NO_3^- are given at the same concentration, and growth may be accelerated despite high energy requirements (Bi et al. 2020). Energy costs do not differ between NO_3^- and NH_4^+ when the assimilation of NO_3^- occurs in the shoots, especially under abiotic stress (Guo et al. 2007). Interestingly, poplar females have a higher specific root length (SRL), which indicates a lower carbon cost but a weaker root exploration capacity compared to males, while lower SRL in males may facilitate the utilization of less-mobile NH_4^+ (Xia et al. 2020). Sex- and N form-dependent root system architecture investments largely reflect energy requirement for foliage construction and, thereby, may affect g_m and photosynthesis. Niinemets (1999) has proposed that the fraction of the annual biomass invested in foliage decreases in older trees, which results from biomass being largely invested in roots and stems. As discussed above, we hypothesize that N forms affect root biomass allocation with further modifications of leaf anatomy and g_m.

In this study, we employ *Populus cathayana* to examine sex-specific adaptive strategies to salt stress under NO_3^- and NH_4^+ supplies with the following hypotheses: (1) sex-specific trade-offs between leaf anatomical properties and g_m determine sex-specific differences in salt adaptation; (2) N forms affect root energy allocation, with further modifications in leaf anatomy and g_m under salt stress in a sex-dependent

manner. This study will not only help us to improve understanding of the response of foliar architecture to photosynthesis under salt stress and different N forms, but it will aid to predict photosynthetic behaviour in tree species with different N source preferences and spatiotemporal changes in N assimilation at rising atmospheric CO_2.

Materials and methods

Plant material and experimental design

Cuttings of *P. cathayana* were obtained from different trees of each sex from populations in riparian and valley flat habitats of the Qinghai Province, China (30° 67′ N, 104° 06′ E), as explained in detail by Liu et al. (2020a). The cuttings were planted in March 2019 at the Hangzhou Normal University, China, (30° 01′ N, 104° 07′ E). The seedlings were cultivated in a semi-controlled greenhouse with a daytime temperature of 21-25 °C, a night-time temperature of 15-18 °C, a photoperiod of 12-14 h, and a relative humidity of 76-81% throughout the growth period. After growing for 5 weeks, 32 uniform and healthy seedlings (16 females and 16 males) with heights of 30-40 cm were transplanted into 10-l plastic pots with a 10-kg mixture of sand, vermiculite and perlite (1:1:1).

The experiment was completely randomized with two sexes (males, females), two N regimes (NO_3^-, NH_4^+), and two NaCl levels (−NaCl, +NaCl). Each treatment was

154 replicated four times. The plants were fertilized every 2 days with 200 ml nutrient
155 solution (pH = 6.0) containing either 3.75 mM NH_4^+ or 3.75 mM NO_3^- as the N
156 source (see Table S1 for the full composition of nutrient solutions). After the seedlings
157 had grown for a further 30 days, half of the cuttings were treated with 200 ml NaCl
158 (200 mM) administered every day until the final NaCl concentration reached 50 mM
159 kg^{-1} growth substrate. Each day, the control cuttings received the same amount of
160 distilled water.
161
162 *Gas exchange and fluorescence measurements*
163
164 Chlorophyll fluorescence and gas exchange characteristics of mature leaves were
165 measured with a portable photosynthesis measuring system (Ll-6400; Li-Cor Inc.,
166 Lincoln, NE, USA) equipped with an integrated leaf chamber fluorometer
167 (LI-6400-40). The measurements were conducted between 09:00 h and 16:30 h. The
168 standard environmental conditions during measurements of leaf photosynthetic
169 characteristics were as follows: leaf temperature of 25 °C, saturating photon quantum
170 flux density (PPFD) of 1200 μmol m^{-2} s^{-1} (with 90% red light and 10% blue light),
171 relative humidity of 75%, air flow rate of 500 μmol s^{-1} and CO_2 concentration in the
172 cuvette (C_a) of 400 μmol mol^{-1}. After leaf gas exchange rates stabilized, typically in
173 20-30 min, the steady-state fluorescence yield (F_s) was recorded, and a saturating
174 light flash of 8000 μmol m^{-2} s^{-1} for 0.8 s was given to measure the maximum
175 fluorescence yield at the light-adapted state (F_m'). For measurements of chlorophyll

fluorescence, leaves were adapted to the dark for 30 min using an aluminium foil cover. The minimum fluorescence (F_o) and maximum fluorescence (F_m) were measured. After these measurements, CO_2 response curves were measured with C_a lowered stepwise from 400 to 300, 200, 100 and 50 μmol mol^{-1}, and then raised from 50 to 400, 600, 800 and 1000 μmol mol^{-1}, while all other environmental conditions were maintained. The chlorophyll fluorescence characteristics, F_S and F_m', were also measured at each C_a.

Estimation of g_m by chlorophyll fluorescence and gas exchange

The photochemical efficiency of photosystem II (Φ_{PSII}) was calculated according to Genty et al. (1989):

$$\Phi_{PSII} = (F_m' - F_s) / F_m' \quad (1)$$

The electron transport rate from chlorophyll fluorescence (J) was calculated as follows:

$$J = \Phi_{PSII} \cdot Q \cdot \alpha \cdot \beta \quad (2)$$

where the product αβ (β is the fraction of light absorbed by PSII, and α is leaf absorptance) is obtained from the correlation between photosynthetic rate (A) and Q

198 •Φ_{PSII}/4 using the light response curve under non-photorespiratory conditions ([O_2] <
199 1.0%) (Yin et al. 2009). The light response curve under low [O_2] was measured based
200 on the method of Lu et al. (2016). *Q* is *PPFD*.
201
202 The CO_2 response curves were used to estimate g_m according to the variable *J* method
203 proposed by Harley et al. (1992); g_m was calculated as follows:
204
205 $$g_m = \frac{A}{C_i - \frac{\Gamma^*(J + 8(A + R_d))}{J - 4(A + R_d)}} \quad (3)$$
206
207 where R_d is the dark respiration rate continuing in light, and Γ^* is the hypothetical
208 CO_2 compensation point in the absence of R_d (Bernacchi et al. 2001, Tosens et al.
209 2012b). Then, g_m was used to transform A/C_i response curves into A/C_c response
210 curves by the equation $C_c = C_i - A/g_m$ and $\Gamma^* = C_i^* + R_d/g_m$. C_c was used to calculate
211 the maximum velocity of carboxylation and the photosynthetic electron transport
212 according to the method of Bernacchi et al. (2002). Each g_m was replicated four times
213 for every specimen. R_d and Ci^* were measured according to Brooks and Farquhar
214 (1985). Briefly, the A/C_i curve was generated at PPFD of 150, 300 and 600 μmol m^{-2}
215 s^{-1}, with each having four C_a chambers (50, 75, 100 and 150 μmol CO_2 mol^{-1}). The
216 x-axis and y-axis of the intersection point of three A/C_i curves represented C_i^* and R_d,
217 respectively.
218
219 *Estimation of leaf construction costs*

Leaf construction costs [CC, g glucose (g dry mass)$^{-1}$] were calculated from ash [g g^{-1}(d.m.)], N [g g^{-1}(d.m.)] and H_c [kJ g^{-1}(d.m.)] according to Williams et al. (1987):

$$CC = \{[(0.06968 \times H_c - 0.065)\ (1 - ash)] + [(K \times N/14.0067)(180.15/24)]\}/0.89 \quad (4)$$

where K is the substrate of nitrogen oxidation state, +5 for nitrate and −3 for ammonium. H_c is the ash-free heat of combustion.

Microscopic observations and anatomical measurements

Leaf segments (1×1 mm) were taken from leaves avoiding major veins, and fixed in a formaldehyde, acetic acid and alcohol solution (1:1:8 v/v) under vacuum for 20 min. Thereafter, the samples were thoroughly washed three times with deionized water and dehydrated in a graded ethanol series. Sections were embedded in glycol methacrylate under vacuum. Semi-thin cross-sections were stained with safranin-fast green and viewed under a light microscope (Nikon Corporation, Kyoto, Japan) at 20× magnification. The following characteristics were measured from light micrographs: the thickness, size and density of leaf palisade and spongy tissues, and the sum of spongy and palisade tissue cell area per transverse section.

In addition, leaf samples were cut and fixed in 4% (v/v) glutaraldehyde in sodium

phosphate buffer (0.2 M, pH = 7.2) overnight. The samples were thoroughly washed three times with a sodium phosphate buffer and then post-fixed in 1% (w/v) osmium tetroxide for 1 h. After dehydration in a graded ethanol series, the samples were immersed in 1:3 (v/v) Spurr's resin and acetone. The dehydrated samples were embedded in Spurr's resin and dried on glass slides. Ultrathin (90 nm) cross sections were stained with 2.0% uranyl acetate (w/v) and lead citrate, and viewed with a transmission electron microscope (H-7650, Hitachi, Tokyo, Japan). Cell wall thickness (T_{cw}), the distance between two neighbouring chloroplasts (ΔL_{chl}), cytoplasm thickness (T_{cyt}), chloroplast distance from the cell wall ($\Delta_{Lcyt,1}$), and chloroplast thickness (T_{chl}) and length (L_{chl}) were measured at 20,000-40,000× magnification. Each anatomical characteristic per specimen was determined from four to six different fields of view for each section and calculated based on the method of Tomás et al. (2013). All photographs were analysed with Image J (Wayne Rasband/NIH, Bethesda, MD, USA).

S_c/S and mesophyll surface area (S_m/S) exposed to intercellular air space per leaf area were calculated as follows:

$$S_c/S = \frac{L_{mes}}{W} F \quad (5)$$

$$S_m/S = \frac{L_c}{L_{mes}} S_m/S \quad (6)$$

where L_c and L_m are the distances of the chloroplast surface area and the mesophyll cells facing the intercellular air space, respectively; W is the width of the measured section; and F is the cell curvature correction factor, which is calculated according to the method of Thain et al. (1983). The values of F ranged from 1.4-1.5 for palisade cells and 1.16−1.4 for spongy cells.

The fraction of intercellular air space (f_{ias}) in leaf mesophyll, f_{ias} was estimated as:

$$f_{ias} = 1 - \frac{\sum S_s}{t_{mes} W} \quad (7)$$

where t_{mes} is mesophyll thickness.

All parameters were analysed at three different fields and at three different sections. The weighted average was calculated based on tissue volume fractions according to Tomás et al. (2013).

Determination of leaf area, leaf dry mass per unit area, and leaf sodium content

Leaf samples were washed three times with deionized water and dried at 75 °C to a constant mass. Dry samples were ground and digested with 3:1 (v/v) HNO_3 and $HClO_4$. Na concentration was determined using inductively coupled plasma mass spectrometry (Agilent 7500a, Agilent Technologies, CA, USA).

286

287 *Quantitative photosynthetic limitation analysis*

288

289 A quantitative limitation analysis was used to distribute the relative controls on A
290 among stomatal limitation (S_L), mesophyll conductance limitation (MC_L) and
291 biochemical limitation (B_L) (Grassi and Magnani 2005), as modified by Tomás et al.
292 2013). The relative changes in photosynthesis are expressed as:

293

294 $$\frac{dA}{A} = S_L + MC_L + B_L = l_s \frac{dg_{sc}}{g_{sc}} + l_{mc} \frac{dg_m}{g_m} + l_b \frac{dV_{cmax}}{V_{cmax}} \quad (8)$$

295

296 $$l_s = \frac{g_{tot}/g_s \cdot \partial A / \partial C_c}{g_{tot} + \partial A / \partial C_c} \quad (9)$$

297

298 $$l_m = \frac{g_{tot}/g_m \cdot \partial A / \partial C_c}{g_{tot} + \partial A / \partial C_c} \quad (10)$$

299

300 $$l_b = \frac{g_{tot}}{g_{tot} + \partial A / \partial C_c} \quad (11)$$

301

302 where l_m, l_s and l_b are the corresponding relative limitations due to g_m, g_s and
303 biochemical capacity (V_{cmax}), respectively; ($l_s + l_m + l_b = 1$). The total CO_2 diffusion
304 conductance, g_{tot}, was given by:

305

306 $$g_{tot} = \frac{1}{1/g_{sc} + 1/g_m} \quad (12)$$

307

308 $\partial A/\partial C_c$ was estimated as the slope of A/C_c curves with the range of C_c at 50-100 μmol
309 mol^{-1} (Tomás et al. 2013). At least three A/C_c curves of each treatment were used, and
310 average values were calculated.
311
312 Relative changes in A, g_m, V_{cmax} and stomatal conductance to CO_2 (g_{sc}) due to the salt
313 treatment were estimated as follows (Chen et al. 2015):
314
315 $$\frac{dA}{A} \approx \frac{A_{max}^{ref} - A}{A_{max}^{ref}} \quad (13)$$
316
317 $$\frac{dg_m}{g_m} \approx \frac{g_m^{ref} - g_m}{g_m^{ref}} \quad (14)$$
318
319 $$\frac{dV_{cmax}}{V_{cmax}} \approx \frac{V_{max}^{ref} - V_{cmax}}{V_{cmax}^{ref}} \quad (15)$$
320
321 $$\frac{dg_{sc}}{g_{sc}} \approx \frac{g_{sc}^{ref} - g_{sc}}{g_{sc}^{ref}} \quad (16)$$
322
323 where g_m^{ref}, g_{sc}^{ref}, A_{max}^{ref} and V_{cmax}^{ref} are the reference (maximum) values of g_m, g_{sc}, A
324 and V_{cmax}, respectively (Grassi and Magnani 2005). The reference values for A, g_{sc}, g_m
325 and V_{cmax} correspond to NO_3^- and NH_4^+ treatments without salt stress.
326
327 The CO_2 liquid-phase diffusion conductance in cytosol, cell wall and stromal

conductance were calculated according to a general formula:

$$g_i = \frac{1}{r_i} = \frac{r_{f,l} \cdot D_w \cdot p_i}{\Delta L_i} \quad (17)$$

where g_i denotes the individual component conductance (r_i is the CO_2 liquid-phase diffusion resistance), and D_w, p_i (m^3 m^{-3}) and ΔL_i (m) are the CO_2 aqueous-phase diffusion coefficient (1.79×10^{-9} m^2 s^{-1} at 25 °C), effective porosity for the given diffusion pathway component and the length of the diffusion path in the corresponding diffusion component, respectively. The dimensionless factor $r_{f,l}$ considers the reduction of diffusion in different cellular components due to the presence of solutes and macromolecules; $r_{f,l}$ was taken as 0.3 for cytosol and stroma, and 1.0 for cell walls (Niinemets and Reichstein 2003, Rondeau-Mouro et al. 2008). The effective porosity was 1.0 for stroma and cytosol. The p_i value of the cell wall was estimated by a least-squares iterative analysis to obtain the best fit between the modelled and measured g_m values (Tosens et al. 2012b, Tomás et al. 2013). The p_i value of the cell wall was set at 0.3 for the thinnest cell walls and 0.028 for the thickest cell walls (Nobel 1991, Tosens et al. 2012b). In this study, the conductance of the chloroplast envelope (g_{env}) and plasma membrane (g_{pl}) was set to 0.0035 m s^{-1} (Tosens et al. 2012a).

The total liquid-phase conductance consisted of two parallel pathways and was calculated as follows (Tomás et al. 2013):

$$g_{liq} = \frac{S_c}{(r_{cw} + r_{pl} + r_{cel,1})} + \frac{S_m - S_c}{(r_{cw} + r_{pl} + r_{cel,2})} \quad (18)$$

where r_{cw}, r_{pl}, $r_{cel,1}$, and $r_{cel,2}$ are the resistances of cell wall, plasma membrane, cell wall parts with chloroplasts and the interchloroplastial areas, respectively (Tomás et al. 2013). The $r_{cel,1}$ and $r_{cel,2}$ were calculated as follows:

$$g_{cel,1} = \frac{1}{r_{cyt,1} + r_{env} + r_{st,1}} \quad (19)$$

$$g_{cel,2} = \frac{1}{r_{cyt,2} + r_{env} + r_{st,2}} \quad (20)$$

where $r_{st,1}$ and $r_{st,2}$ are the stromal resistance perpendicular and parallel to the cell walls, respectively. The $r_{cyt,1}$ value is defined as the CO_2 resistance through the plasmalemma inner surface to the outer surface of chloroplasts, and $r_{cyt,2}$ as the resistance from interchloroplastic cell wall portions to the outer surface of chloroplasts (Tomás et al. 2013). These equations give g_m in m s^{-1}. The conversion to molar units is given as follows:

g_m [mol m^{-2} s^{-1}] = g_m [m s^{-1}] 44.6 [273.16/(273.16 + T)(P/101325)], where T is leaf temperature in ^oC and P is air pressure in Pa.

Quantitative analyses of anatomical limitations of g_m

The quantitative contributions of different anatomical traits to g_m were separated according to Tosens et al. (2012b) and Tomás et al. (2013). The share of g_m in the gas phase was calculated as follows:

$$l_{ias} = \frac{g_m}{g_{ias}} \quad (21)$$

The limitations of g_m by different liquid-phase components (l_i, where i stands for a diffusion pathway component, including cell wall, cytosol, chloroplast stroma, chloroplast envelope and plasmalemma) were calculated as follows:

$$l_i = \frac{g_m}{g_i \frac{S_m}{S}} \quad (22)$$

where g_i is the corresponding CO_2 conductance of the diffusion pathway.

Estimation of g_m by a curve-fitting method

Estimation of g_m was performed by the method of Ethier and Livingston (2004). The g_m estimation was performed with the A/C_i curves with a non-rectangular hyperbola version of the Farquhar's biochemical model for leaf photosynthesis (Farquhar et al. 1980). The g_m value from the fitting of A/C_i and measured from combined gas exchange (g_m) and chlorophyll fluorescence measurements (g_m-gas exchange) were

significantly correlated ($r^2 = 0.79$, $P < 0.05$; Figure S1).

Statistical analyses

Statistical analyses were conducted using the SPSS software (version 22.0). Before analyses of variance (ANOVAs), the data were checked for normality. The differences between mean values were compared by Duncan's tests at a significance level of $P < 0.05$. Three-way analyses of variance were performed to examine the effects of sex, N forms and salt levels. Structural equation modeling was used to evaluate the indirect and direct relationships between leaf structure, biomass allocation, chloroplast exposed surface to leaf area ratio (S_c/S), mesophyll cell area per transverse section width (S/W), CO_2 mesophyll conductance (g_m) and photosynthesis (A). Before the construction of the structure equation modeling, we conducted a principal component analysis (PCA) to create the multivariate functional index due to the correlations among the factors within each group. The structural equation modeling analyses were performed using the R package "lavaan" v. 0.6−1 (Rosseel 2012).

Results

Morphological and anatomical traits of leaves

Salt stress significantly decreased leaf A, g_m, g_s, leaf area, leaf biomass, F_v/F_m,

chlorophyll concentration, the rate of photosynthetic electron transport (J, Eq. 2) and V_{cmax} in females and males grown under both N forms (except for F_v/F_m under NH_4^+ supply and leaf biomass under both N forms in males). The salt effects were greater in females than in males (Figure 1; Table 1; Table S2). Salt stress increased leaf dry mass per unit area (*LMA*) and leaf thickness (Figure 1; Table 1). Compared with control conditions, salt stress increased *LMA* by 37% and 59% in females, and by 21% and 16% in males under NO_3^- and NH_4^+ supply, respectively. Leaf thickness increased by 59% and 56% in females, and by 26% and 19% in males by salt stress under NO_3^- and NH_4^+ supply, respectively (Table 2). The leaf construction cost with salt stress exposure was slightly higher in males than in females under NH_4^+ supply, but it was similar in both sexes under NO_3^- supply (Table 1). The leaf dark respiration rate (R_d) increased by salt stress, and the effect of salt stress on R_d was greater in females than in males under both N forms. Salt stress induced R_d more in females under NO_3^- supply than under NH_4^+ supply; there was no significant difference in R_d in males between the two N forms (Table S2). The SRL value in females was greater than that in males, and the increase in SRL was more significant under NO_3^- supply in males (Table 1). The contrary was true for root length density (RLD) under salt stress. The root biomass and the ratio of root to shoot were higher in females than in males with salt stress under both N forms (Table 1; Table S2).

The density of both mesophyll palisade and spongy tissue cells was higher in females than in males exposed to salt stress under both N forms (Table S2). The contrary was

true for the thickness of palisade and spongy tissues. Palisade and spongy cells were denser in NH_4^+-fed females than in those supplied by NO_3^- under salt stress, while a higher density of palisade and spongy cells was found in males with NO_3^- supply under salt stress (Table S2). Leaf thickness, f_{ias}, S_m/S, S_c/S, and chloroplast density and length were higher in males than in females with salt stress under both N forms (Table 2). NH_4^+-fed males with salt stress had lower S/W and chloroplast density but higher f_{ias} under NO_3^- supply (Table 2). In contrast, there was no significant difference in leaf thickness, S_m/S, S/W, or chloroplast density and length in females with salt stress under either N form, but S_c/S and f_{ias} were lower under NH_4^+ supply (Table 2). T_{cw}, T_{chl}, $l_{cyt,1}$ and $l_{cyt,2}$ in salt-stressed plants were higher under NO_3^- and NH_4^+ supply in both sexes compared with control plants (Figure 1; Table 2). In males, salt stress increased T_{cw}, T_{chl}, $l_{cyt,1}$ and $l_{cyt,2}$ by 23%, 15%, 43% and 20%, respectively, under NO_3^- supply, and by 15%, 24%, 66% and 28%, respectively, under NH_4^+ supply (Table 2). In contrast, in females, T_{cw}, T_{chl}, $l_{cyt,1}$,and $l_{cyt,2}$ increased by 19%, 34%, 62% and 37%, respectively, under NO_3^- supply, and by 29%, 40%, 32% and 39%, respectively, under NH_4^+ supply in salt-stressed plants (Table 2).

Correlations of g_m with physiological characteristics of leaves

The net photosynthesis rate (A) exhibited a significant positive correlation with g_m and g_s in both sexes under both NO_3^- and NH_4^+ supply (Figure 2a, b). Under both N forms, A at a given g_s and g_m was higher in males than in females irrespective of salt stress

460 (Figure 2, $P < 0.05$, Duncan's test), reflecting a greater photosynthetic capacity in
461 males. With an increasing Na^+ concentration in leaves, g_m decreased significantly in
462 both sexes, especially in males under NH_4^+ supply (Figure 2c). Both g_m and the CO_2
463 drawdown from intercellular air space to chloroplasts (C_i-C_c) decreased under salt
464 stress, but the reductions were greater in females than in males, especially under NH_4^+
465 supply (Figure 2d).
466
467 *Correlations of g_m with anatomical traits of leaves*
468
469 Strong positive correlations between g_m and f_{ias} were observed in females and males
470 under all treatments ($P < 0.001$, Duncan's test) (Figure 3a). In males, f_{ias} decreased by
471 salt stress more under NO_3^- than under NH_4^+ supply, whereas lower f_{ias} was observed
472 under NH_4^+ than under NO_3^- supply (Figure 3a). According to multiple regression
473 analyses, g_m was positively associated with S_m/S and S_c/S in all treatments in both
474 sexes ($P < 0.001$; Duncan's test, Figure 3b, c). At given S_m/S, g_m was greater in males
475 than in females, but a similar relationship between g_m and S_c/S was observed in both
476 sexes (Figure 3b, c). A strong negative relationship was observed between g_m and T_{cw}
477 in both sexes under both N forms ($P < 0.001$; Duncan's test, Figure 3d). The slopes of
478 g_m vs. T_{cw} were similar in males and females, but because salt stress led to higher T_{cw}
479 in females than in males (see above), the g_m vs. T_{cw} line was shifted towards higher
480 T_{cw} values along the common slope (Figure 3d). S_c/S and T_{cw} better explained the
481 sexually differential g_m relative to f_{ias} and S_m/S. In contrast, f_{ias} and S_m/S explained the

differences among treatments for each sex.

Limitation of photosynthesis under salt stress

According to the quantitative limitation analysis, salt stress changed the share of mesophyll, stomatal and biochemical limitations in both sexes under NH_4^+ and NO_3^- supply (Figure 4a). In particular, biochemical and mesophyll diffusion limitations (Eqs 10-11) restricted photosynthetic capacity more than stomatal limitations (Eq. 9) under salt stress (Figure 4a). Mesophyll diffusion limitations due to salt stress were higher in females than in males under both N forms, and the extent of inhibition due to salt stress was greater under NH_4^+ than under NO_3^- supply (Figure 4a). Salt stress strongly increased biochemical limitations in females under both N forms, but the extent of such limitations was more significant in males under NO_3^- than under NH_4^+ supply. Stomatal limitations were higher under NO_3^- than under NH_4^+ supply, especially in females (Figure 4a, $P < 0.05$, Duncan's test). Positive relationships were observed between leaf Na and S_L, and Na and MC_L in both sexes (Figure 4b).

Limitations of g_m resulting from diffusion pathway components

In all cases, CO_2 liquid phase diffusion represented a higher proportion of the total diffusion pathway limitation than did gas phase diffusion (Figure 5a-d). For the liquid phase, decreases in the absolute values of CO_2 diffusion conductance due to salt stress

were greater in females than in males under both N forms (Figure 5d). Moreover, the salt stress-dependent increase in the absolute liquid phase conductance was lower under NH_4^+ than under NO_3^- supply in females but not in males (Figure 5d).

The analysis of different liquid phase components indicated that the chloroplast stroma and cytoplasm were the most limiting components in females and males (Figure 6a, b). In salt-stressed females, the share of overall limitation due to chloroplast stroma was reduced under NH_4^+ but unaffected under NO_3^- supply. In contrast, salt stress increased the CO_2 diffusion limitation due to cytoplasm in both sexes. Salt stress did not affect chloroplast stromal limitation under either N form in males (Figure 6a, b). The limitation of liquid phase conductance due to cell walls was not affected by salt stress under either N supply in either sex. However, salt stress led to 43% and 109% increases in the relative chloroplast envelope limitation under NO_3^- and NH_4^+ supply, respectively, in females, while the limitation of the chloroplast envelope did not change by salt stress in males under NH_4^+ supply (Figure 6a, b).

The absolute values of diffusion conductance differed among sexes and treatments (Figure 6c, d). Salt stress decreased g_{cyt1}, g_{cyt2} and g_{st1} in both sexes under NO_3^- and NH_4^+ supply, and the effects of salt stress on cytoplasm conductance were greater in males than in females (Figure 6c, d; Figure S2). The g_{st2} value of females also decreased by salt stress under NH_4^+ supply, but there was no significant difference in males under either N form (Figure 6c, d; Figure S2). Compared with control

conditions, salt stress had higher g_{st1} and g_{cw}, and lower g_{cyt1} in females under NO_3^- than under NH_4^+ supply, whereas no significant differences were found in g_{st2} and g_{cyt2} values between the two N forms (Figure S2). In males, greater g_{cw} and g_{st2}, and lower g_{cyt1} and g_{cyt2} induced by salt stress were found under NH_4^+ supply than under NO_3^- supply (Figure 6c, d; Figure S2). There was no significant difference in g_{st1} between the two N forms in males.

Structural equation modelling

As shown in Figure 7, structural equation modelling suggested that leaf S/W and g_m had direct effects on leaf photosynthesis (r^2 = −0.49 and 0.51, respectively). The leaf photosynthesis was positively correlated with leaf g_m but negatively correlated with leaf S/W. Leaf S_c/S had a direct positive effect on g_m (r^2 = 0.41), while leaf S/W had a direct negative effect on g_m (r^2 = −0.60). Leaf structure had a direct positive effect on biomass allocation (r^2 = 0.47) and S/W (r^2 = 0.34), but a direct negative effect on S_c/S (r^2 = −0.30). By contrast, biomass allocation had a direct positive effect on S_c/S (r^2 = 0.36).

Schematic modes showing the sexual difference in g_m

As shown in Figure 8, under salt stress, females had less chloroplast and more mesophyll spongy cells; the contrary was true for males under both N forms. The CO_2

548 stroma (g_{st}) and cytoplasm conductance (g_{cyt}) were the lowest among the CO_2 liquid
549 conductance levels. The CO_2 cell wall conductance of females was lower with NH_4^+
550 supply, but lower with NO_3^- supply when compared to males under salt stress. The
551 g_{st1} and g_{cyt1} values of males were higher than those of females under both N forms
552 and salt stress. Under salt stress, g_{st2} was higher in females than in males with NH_4^+
553 supply, but it showed no significant difference between the sexes under NO_3^- supply.
554 NH_4^+-fed females had greater g_{cyt1} but lower g_{st1} and g_{cw}, and similar g_{st2} and g_{cyt2} than
555 those under NO_3^- supply, while males had higher g_{cyt1} and g_{cyt2}, lower g_{cw} and g_{st2},
556 and similar g_{st1} under NO_3^- supply than under NH_4^+ supply under salt stress (Figure
557 8).
558
559 **Discussion**
560
561 The present study clearly demonstrated that salt stress imposes sex-specific restraints
562 on CO_2 assimilation, mainly deriving from the restraint of g_m relative to g_s under
563 NO_3^- and NH_4^+ supply. Generally, stomatal closure is the first response to salt stress
564 in plants (Wang et al. 2018). Salt stress could disturb stomatal function, leading to a
565 decreased photosynthetic capacity (Tavakkoli et al. 2011, Pérez-López et al. 2012,
566 Chen et al. 2015). Improving stomatal regulation has been regarded as the most
567 effective approach to alleviate salt stress in plants (Chen et al. 2015, Qiu and Katul
568 2020). In this study, both g_m and g_s were positively correlated with A in females and
569 males under both N forms (Figure 2). The relationship of g_m and g_s was stronger in

females than in males (Figure S3). However, we found that the g_m, g_s and J significantly decreased by salt stress under both N forms, especially in females (Table 1; Table S2).

The variable g_m was the main limiting factor for the sexual difference in A under salt stress. This result was a little inconsistent with a previous study on *Ziziphus spina-christi* trees suggesting that g_m plays a critical role in controlling A only under severe salinity stress (Zait et al. 2019). This could be explained by the different way of calculating l_s and l_m, as well as by the plant species. In the study by Zait et al. (2019), the authors investigated drought-tolerant *Ziziphus spina-christi* trees, which exhibited strong tolerance to salt stress. The concentration of NaCl used in our study was moderate for males but not for females. In this study, the net photosynthetic rate A and stomatal conductance g_s decreased by salt stress more significantly in *Populus cathayana* females than in males. Additionally, g_s was dynamic and changed in response to environmental conditions rapidly or even faster than g_m (Flexas et al. 2008). These results suggested that the photosynthetic limitation from g_m might be higher than that from g_s under our experimental conditions.

Salt stress affects those morphological and anatomical traits of leaves that are associated with CO_2 diffusion into the leaves and leaf photosynthesis (Wankhade et al. 2013, Wang et al. 2018). A higher *LMA* value is correlated with a greater dry mass investment and it has a negative effect on g_m (Tomás et al. 2013, Onoda et al. 2017). Consistently, females with higher *LMA* had lower g_m under salt stress (Table 1). It is

592 noteworthy that males with higher A and g_m had higher *LMA* than females, which
593 suggested that it was not possible to precisely determine g_m and A only from leaf *LMA*
594 (Figure 7), because of the effects of the chemical composition of leaves (John et al.
595 2017). The *S*/*W* value included the total cell area of palisade and spongy tissues per
596 transverse section width, representing the leaf structural investment per area, which
597 would be a more advantageous and convenient trade-off between the leaf structure
598 and photosynthesis (Hu et al. 2020). The results of the structural equation modelling
599 suggested that *S*/*W* plays a critical role in determining g_m and A ($r^2 = -0.60$ for g_m and
600 −0.49 for A) (Figure 7). A lower chloroplast density and a greater mesophyll spongy
601 density in females would reduce light energy capture and CO_2 diffusion conductance
602 in leaves, especially under NH_4^+ supply (Table 2).
603
604 Cell wall thickness and chloroplast distribution are critical fort setting g_m limitation in
605 plants (Terashima et al. 2011). Consistently, S_c/S and T_{cw} were those anatomical
606 variables that best explain differences in g_m between sexes (Figures 3, 7, 8). A greater
607 increase in chloroplast numbers observed in males compared to females facilitated an
608 increase in S_c/S (Figure 8). Higher S_c/S and a lower cell wall thickness led to an
609 increased CO_2 diffusion conductance into male leaves, which was consistent with
610 previous studies (Peguero-Pina et al. 2017, Wang et al. 2018). Indeed, the
611 quantification of g_m limitation showed that g_{cyt} was higher in females than in males
612 during salt stress under both types of N supplies (Figure 6). The proportion of g_{cyt} in
613 the CO_2 diffusion conductance increases along with a reduced contact between

chloroplasts and cell surfaces (Lu et al. 2016). Modifications in the chloroplast shape and structure affect the distance of cytosolic CO_2 diffusion under abiotic stress (Shu et al. 2012). Changes in the shape of female chloroplasts caused by salt stress probably decreased the g_{cyt} value and, thus. g_m as well.

Generally, the distance has little effect on CO_2 diffusion when the cellular stromal distance between the plasma membrane and chloroplast envelope is relatively short. However, intracellular CA could convert CO_2 into HCO_3^-, having the highest activity in the stroma and, thus, affecting g_m (Evans et al. 2009). The effects of N forms on g_{st} and g_{cyt} were sex-dependent under salt stress. NH_4^+-fed females had greater g_{cyt1} but lower g_{cw} and g_{st1} than those under NO_3^- supply, while males had higher g_{cw} and lower g_{st2} under NH_4^+ than under NO_3^- supply (Figures 6, 8; Figure S2). Additionally, nitrogen availability and forms have been found to affect CA activities under salt stress (Siddiqui et al. 2010, Nawaz et al. 2020). Therefore, CA may increase its effect on g_m inside chloroplasts. In addition, increasing evidence suggests that aquaporins are capable of transporting CO_2 in plants and the aquaporin activity is associated with g_m in leaves (Maurel et al. 2008, Heckwolf et al. 2011). Some studies have suggested that salt stress or nitrogen availability increase aquaporin activities (Qi et al. 2009), which indicates that the variation in aquaporin activities under salt stress and N availability might partially affect g_m.

The effects of N forms on g_m and A largely depend on salt stress tolerance and the

636 energy allocation of plants. N forms affect matter distribution and carbohydrate
637 consumption in plants (Guo et al. 2007, Ashraf et al. 2018). A greater investment in
638 the leaf area and cell wall thickness results in a lower allocation of resources to leaf
639 photosynthesis in females. Net photosynthesis could be reduced not only by a greater
640 energy investment in structures but also by higher maintenance costs, including the
641 effects of abiotic stresses (Guo et al. 2007). Females show a higher respiration rate
642 than males under drought stress in *Populus cathayana* (Han et al. 2013). The higher
643 dark respiration rate in *P. cathayana* females under salt stress found in the present
644 study was probably associated with the leaf photosynthesis (Table S2). NO_3^-
645 assimilation in plants requires more energy than NH_4^+ assimilation, while carbon
646 losses through leaf and root respiration are higher under NH_4^+ than under NO_3^- supply.
647 Whether or how N assimilation in plants affects photosynthesis under salt stress was
648 not clear. In the future, it will be important to clarify the sexually different leaf
649 photosynthesis under salt stress with different N form supplies based on the
650 relationship between photosynthesis and respiration consumption.
651
652 Importantly, the sex- and N form-specific investment in the root system architecture
653 largely reflects energy requirements for foliage construction, thereby, affecting g_m and
654 photosynthesis. In this study, the biomass allocation did not directly explain leaf *A*,
655 whereas the biomass allocation had indirect effects on leaf *A* through leaf structural
656 traits (Figure 7). NH_4^+-fed males with a higher root biomass had high root
657 construction costs, while NO_3^--fed males with a higher leaf biomass had high energy

cost from NO_3^- assimilation without salt stress. Such energy trade-offs between biomass and A in males led to similar g_m and photosynthesis under both N forms. Females produce thinner roots than males and they intensively facilitate the exploration of thesurrounding soil and Na^+ uptake (Xia et al. 2020). Certainly, the larger root system and ion uptake enhanced the energy consumption of females exposed to salt stress, especially under NH_4^+ supply.

Conclusions

This study suggested that leaf g_m relative to g_s under salt stress was the main restraint on leaf A under NO_3^- and NH_4^+ supplies. Among leaf structural components, S_c/S and S/W were critical factors affecting g_m and A (Figure 7). Salt stress increased S/W, and reduced intercellular air space and S_c/S, resulting in an increased length of cytoplasmic and stromal paths, and inhibition of g_m and A in females (Figure 8). Conversely, males had a better tradeoff between leaf structure and photosynthesis (more chloroplasts and fewer spongy cells), and they have a good ability to regulate leaf CO_2 diffusion and light capture into the leaf, thereby alleviating g_m and A decreases under salt stress and both N forms (Figure 8). The low CO_2 diffusion conductance in NH_4^+-fed females was mainly due to g_{st1} and g_{cw}, while NO_3^--fed males had a higher cytoplasm conductance (Figure 8). Moreover, biomass allocation in both sexes indirectly affected leaf structural traits and A under both N forms. This study will not only help us to predict potential climate change impacts on dioecious *P.*

cathayana populations, but also to predict the photosynthetic behavior of tree species with different N-source preferences and spatiotemporal changes in N assimilation at rising atmospheric CO_2.

Acknowledgements This work was supported by the Natural Science Foundation of China (31800507) and the Talent Program of the Hangzhou Normal University (2016QDL020).

Author contributions Miao Liu had the main responsibility for data collection, analysis and writing, Xiucheng Liu and Xuhua Du contributed to data analysis, Helena Korpelainen and Ülo Niinemets contributed to the interpretation of data and manuscript preparation, and Chunyang Li (the corresponding author) had the overall responsibility for the experimental design and project management.

Conflict of interest The authors declare that they have no conflict of interest.

References

Ashraf M, Shahzad SM, Imtiaz M, Rizwan MS, Arif MS, Kausar R (2018) Nitrogen nutrition and adaptation of glycophytes to saline environment: a review. Arch Agron Soil Sci 64:1181-1206.

Berghuijs HN, Yin X, Ho QT, Driever SM, Retta MA, Nicolaï BM, Struik PC (2016) Mesophyll conductance and reaction-diffusion models for CO_2 transport in C_3 leaves; needs, opportunities and challenges. Plant Sci 252:62-75.

Bernacchi CJ, Singsaas EL, Pimentel C, Portis Jr AR, Long SP (2001) Improved temperature response functions for models of Rubisco-limited photosynthesis. Plant Cell Environ 24:253-259.

Bernacchi CJ, Portis AR, Nakano H, Von Caemmerer S, Long SP (2002) Temperature response of mesophyll conductance. Implications for the determination of Rubisco enzyme kinetics and for limitations to photosynthesis in vivo. Plant Physiol 130:1992-1998.

Bi J, Liu X, Liu S, Wang Y, Liu M (2020) Microstructural and physiological responses to cadmium stress under different nitrogen forms in two contrasting *Populus* clones. Environ Exp Bot 169:103897.

Brooks A, Farquhar GD (1985) Effect of temperature on the CO_2/O_2 specificity of ribulose-1, 5-bisphosphate carboxylase/oxygenase and the rate of respiration in the light. Planta 165:397-406.

Cano FJ, Sánchez-Gómez D, Rodríguez‐Calcerrada J, Warren CR, Gil L, Aranda I (2013) Effects of drought on mesophyll conductance and photosynthetic

717 limitations at different tree canopy layers. Plant Cell Environ 36:1961-1980.
718 Chen J, Duan B, Xu G, Korpelainen H, Niinemets Ü, Li C (2016) Sexual competition
719 affects biomass partitioning, carbon–nutrient balance, Cd allocation and
720 ultrastructure of *Populus cathayana* females and males exposed to Cd stress. Tree
721 Physiol 36:1353-1368.
722 Chen L, Han Y, Jiang H, Korpelainen H, Li C (2011) Nitrogen nutrient status induces
723 sexual differences in responses to cadmium in *Populus yunnanensis*. J Exp Bot
724 62:5037-5050.
725 Chen TW, Kahlen K, Stützel H (2015) Disentangling the contributions of osmotic and
726 ionic effects of salinity on stomatal, mesophyll, biochemical and light limitations
727 to photosynthesis. Plant Cell Environ 38:1528-1542.
728 Ethier GJ, Livingston NJ (2004) On the need to incorporate sensitivity to CO_2 transfer
729 conductance into the Farquhar-von Caemmerer-Berry leaf photosynthesis model.
730 Plant Cell Environ 27:137-153.
731 Evans JR, Kaldenhoff R, Genty B, Terashima I (2009) Resistances along the CO_2
732 diffusion pathway inside leaves. J Exp Bot 60:2235-2248.
733 Farquhar GD, von Caemmerer SV, Berry JA (1980) A biochemical model of
734 photosynthetic CO_2 assimilation in leaves of C_3 species. Planta 149:78-90.
735 Flexas J, Díaz-Espejo A, Conesa MA, Coopman R, Douthe C, Gago J, Gallé A,
736 Galmés J, Medrano H, Ribas-Carbo M, Tomàs M, Niinemets Ü (2016) Mesophyll
737 conductance to CO_2 and Rubisco as targets for improving intrinsic water use
738 efficiency in C_3 plants. Plant Cell Environ 39:965-982.

739 Flexas J, Ribas-Carbo MI, Diaz-Espejo AN, GalmES J, Medrano H (2008) Mesophyll
740 conductance to CO_2: current knowledge and future prospects. Plant Cell Environ
741 31:602-621.
742 Genty B, Briantais JM, Baker NR (1989) The relationship between the quantum yield
743 of photosynthetic electron transport and quenching of chlorophyll fluorescence.
744 BBA-Gen Subjects 990:87-92.
745 Golldack D, Li C, Mohan H, Probst N (2014) Tolerance to drought and salt stress in
746 plants: unraveling the signaling networks. Front Plant Sci 5:151.
747 Grassi G, Magnani F (2005) Stomatal, mesophyll conductance and biochemical
748 limitations to photosynthesis as affected by drought and leaf ontogeny in ash and
749 oak trees. Plant Cell Environ 28:834-849.
750 Guo S, Zhou Y, Shen Q, Zhang F (2007) Effect of ammonium and nitrate nutrition on
751 some physiological processes in higher plants-growth, photosynthesis,
752 photorespiration, and water relations. Plant Biol 9:21-29.
753 Han Y, Wang Y, Jiang H, Wang M, Korpelainen H, Li C (2013) Reciprocal grafting
754 separates the roles of the root and shoot in sex-related drought responses in
755 *Populus cathayana* males and females. Plant Cell Environ 36:356-364.
756 Harley PC, Thomas RB, Reynolds JF, Strain BR (1992) Modelling photosynthesis of
757 cotton grown in elevated CO_2. Plant Cell Environ 15:271-282.
758 Heckwolf M, Pater D, Hanson DT, Kaldenhoff R (2011) The *Arabidopsis thaliana*
759 aquaporin AtPIP1; 2 is a physiologically relevant CO_2 transport facilitator. Plant J
760 67:795-804.

761 Henry DA, Simpson RJ, Macmillan RH (2000) Seasonal changes and the effect of
762 temperature and leaf moisture content on intrinsic shear strength of leaves of
763 pasture grasses. Aust J Agr Res 51:823-831.
764 Hu W, Lu Z, Meng F, Li X, Cong R, Ren T, Sharkey TD, Lu J (2020) The reduction in
765 leaf area precedes that in photosynthesis under potassium deficiency: the
766 importance of leaf anatomy. New Phytol. https://doi.org/10.1111/nph.16644.
767 John GP, Scoffoni C, Buckley TN, Villar R, Poorter H, Sack L (2017) The anatomical
768 and compositional basis of leaf mass per area. Ecol Lett 20:412-425.
769 Liu M, Bi J, Liu X, Kang J, Korpelainen H, Niinemets Ü, Li C (2020a)
770 Microstructural and physiological responses to cadmium stress under different
771 nitrogen levels in *Populus cathayana* females and males. Tree Physiol 40:30-45.
772 Liu M, Liu X, Kang J, Korpelainen H, Li C (2020b) Are males and females of
773 *Populus cathayana* differentially sensitive to Cd stress? J Hazard Mater
774 393:122411.
775 Liu M, Wang Y, Liu X, Korpelainen H, Li C (2021) Intra-and intersexual interactions
776 shape microbial community dynamics in the rhizosphere of *Populus cathayana*
777 females and males exposed to excess Zn. J Hazard Mater 402:123783.
778 Lu Z, Lu J, Pan Y, Lu P, Li X, Cong R, Ren T (2016) Anatomical variation of
779 mesophyll conductance under potassium deficiency has a vital role in determining
780 leaf photosynthesis. Plant Cell Environ 39:2428-2439.
781 Martins SC, Galmes J, Cavatte PC, Pereira LF, Ventrella MC, Damatta FM (2014)
782 Understanding the low photosynthetic rates of sun and shade coffee leaves:

783 bridging the gap on the relative roles of hydraulic, diffusive and biochemical
784 constraints to photosynthesis. Plos One 9:e95571.
785 Maurel C, Verdoucq L, Luu DT, Santoni V (2008) Plant aquaporins: membrane
786 channels with multiple integrated functions. Annu Rev Plant Biol 59:595-624.
787 Nawaz F, Shehzad MA, Majeed S, Ahmad KS, Aqib M, Usmani MM, Shabbir RN
788 (2020) Role of mineral nutrition in improving drought and salinity tolerance in
789 field crops. Agronomic Crops 129-147.
790 Niinemets U (2007) Photosynthesis and resource distribution through plant canopies.
791 Plant Cell Environ 30:1052-1071.
792 Niinemets Ü (1999) Research review. Components of leaf dry mass per area-
793 thickness and density-alter leaf photosynthetic capacity in reverse directions in
794 woody plants. New Phytol 144:35-47.
795 Niinemets Ü, Díaz-Espejo A, Flexas J, Galmés J, Warren CR (2009b) Role of
796 mesophyll diffusion conductance in constraining potential photosynthetic
797 productivity in the field. J Exp Bot 60:2249-2270.
798 Niinemets Ü, Keenan TF (2014) Photosynthetic responses to stress in Mediterranean
799 evergreens: mechanisms and models. Environ Exp Bot 103:24-41.
800 Niinemets Ü, Reichstein M (2003) Controls on the emission of plant volatiles through
801 stomata: a sensitivity analysis. J Geophys Res-Atmos 108:4211.
802 Niinemets Ü, Wright IJ, Evans JR (2009a) Leaf mesophyll diffusion conductance in
803 35 Australian sclerophylls covering a broad range of foliage structural and
804 physiological variation. J Exp Bot 60:2433-2449.

805 Nobel PS (1991) Physicochemical and environmental plant physiology, 4th edn. San
806 Diego, CA: Academic Press.
807 Onoda Y, Wright IJ, Evans JR, Hikosaka K, Kitajima K, Niinemets Ü, Poorter H,
808 Tosens T, Westoby M (2017) Physiological and structural tradeoffs underlying the
809 leaf economics spectrum. New Phytol 214:1447-1463.
810 Ort DR, Merchant SS, Alric J, Barkan A, Blankenship RE, Bock R, Moore TA (2015)
811 Redesigning photosynthesis to sustainably meet global food and bioenergy
812 demand. P Natl Acad Sci USA 112:8529-8536.
813 Peguero-Pina JJ, Sisó S, Flexas J, Galmés J, García-Nogales A, Niinemets Ü,
814 Sancho-Knapik D, Saz MÁ, Gil-Pelegrín E (2017) Cell -level anatomical
815 characteristics explain high mesophyll conductance and photosynthetic capacity in
816 *sclerophyllous Mediterranean* oaks. New Phytol 214:585-596.
817 Pérez-López U, Robredo A, Lacuesta M, Mena-Petite A, Munoz-Rueda A (2012)
818 Elevated CO_2 reduces stomatal and metabolic limitations on photosynthesis
819 caused by salinity in *Hordeum vulgare*. Photosynth Res 111:269-283.
820 Pinheiro C, Chaves MM (2011) Photosynthesis and drought: can we make metabolic
821 connections from available data? J Exp Bot 62:869-882.
822 Praxedes SC, De Lacerda CF, DaMatta FM, Prisco JT, Gomes-Filho E (2010) Salt
823 tolerance is associated with differences in ion accumulation, biomass allocation
824 and photosynthesis in cowpea cultivars. J Agron Crop Sci 196:193-204.
825 Qi CH, Chen M, Song J, Wang BS (2009) Increase in aquaporin activity is involved in
826 leaf succulence of the euhalophyte *Suaeda salsa*, under salinity. Plant Sci

827 176:200-205.
828 Qiu R, Katul GG (2020) Maximizing leaf carbon gain in varying saline conditions: An
829 optimization model with dynamic mesophyll conductance. Plant J 101:543-554.
830 Ren T, Weraduwage SM, Sharkey TD (2019) Prospects for enhancing leaf
831 photosynthetic capacity by manipulating mesophyll cell morphology. J Exp Bot
832 70:1153-1165.
833 Rondeau-Mouro C, Defer D, Leboeuf E, Lahaye M (2008) Assessment of cell wall
834 porosity in *Arabidopsis thaliana* by NMR spectroscopy. Inter J Biol Macromol
835 42:83-92.
836 Rosseel Y (2012) Lavaan: An R package for structural equation modeling and more.
837 Version 0.5-12 (BETA). J Stat Softw 48:1-36.
838 Siddiqui MH, Mohammad F, Khan MN, Al-Whaibi MH, Bahkali AH (2010) Nitrogen
839 in relation to photosynthetic capacity and accumulation of osmoprotectant and
840 nutrients in Brassica genotypes grown under salt stress. Agr Sci China 9:671-680.
841 Scoffoni C, Sack L, Ort D (2017) The causes and consequences of leaf hydraulic
842 decline with dehydration. J Exp Bot 68:4479-4496.
843 Shu S, Yuan LY, Guo SR, Sun J, Liu CJ (2012) Effects of exogenous spermidine on
844 photosynthesis, xanthophyll cycle and endogenous polyamines in cucumber
845 seedlings exposed to salinity. Afr J Biotechnol 11:6064-6674.
846 Tavakkoli E, Fatehi F, Coventry S, Rengasamy P, McDonald GK (2011) Additive
847 effects of Na^+ and Cl^- ions on barley growth under salinity stress. J Exp Bot
848 62:2189-2203.

849 Terashima I, Hanba YT, Tholen D, Niinemets Ü (2011) Leaf functional anatomy in
850 relation to photosynthesis. Plant Physiol 155:108-116.
851 Thain JF (1983) Curvature correlation factors in the measurements of cell surface
852 areas in plant tissues. J Exp Bot 34:87-94.
853 Tomás M, Flexas J, Copolovici L, Galmés J, Hallik L, Medrano H, Niinemets Ü
854 (2013) Importance of leaf anatomy in determining mesophyll diffusion
855 conductance to CO_2 across species: quantitative limitations and scaling up by
856 models. J Exp Bot 64:2269-2281.
857 Tosens T, Nishida K, Gago J, Coopman RE, Cabrera HM, Carriquí M, Talts E (2016)
858 The photosynthetic capacity in 35 ferns and fern allies: mesophyll CO_2 diffusion
859 as a key trait. New Phytol 209:1576-1590.
860 Tosens T, Niinemets Ü, Vislap V, Eichelmann H, Castro-Diez P (2012a)
861 Developmental changes in mesophyll diffusion conductance and photosynthetic
862 capacity under different light and water availabilities in *Populus tremula*: how
863 structure constrains function. Plant Cell Environ 35:839-856.
864 Tosens T, Niinemets Ü, Westoby M, Wright IJ (2012b) Anatomical basis of variation
865 in mesophyll resistance in eastern Australian sclerophylls: news of a long and
866 winding path. J Exp Bot 63:5105-5119.
867 Veromann-Jürgenson L-L, Tosens T, Brodribb TJ, Niinemets Ü (2020) Pivotal role of
868 mesophyll conductance in shaping photosynthetic performance across 67
869 structurally diverse gymnosperm species. Inter J Plant Sci 181:116-128.
870 Wankhade SD, Cornejo MJ, Mateu-Andrés I, Sanz A (2013) Morpho-physiological

871 variations in response to NaCl stress during vegetative and reproductive
872 development of rice. Acta Physiol Plant 35:323-333.
873 Wang X, Du T, Huang J, Peng S, Xiong D (2018) Leaf hydraulic vulnerability triggers
874 the decline in stomatal and mesophyll conductance during drought in rice. J Exp
875 Bot 69:4033-4045.
876 Williams K, Percival F, Merino J, Mooney HA (1987) Estimation of tissue
877 construction cost from heat of combustion and organic nitrogen content. Plant Cell
878 Environ 10:725-734.
879 Xia ZC, He Y, Yu L, Lv RB, Korpelainen H, Li CY (2020) Sex-specific strategies of
880 phosphorus acquisition in *Populus cathayana* as affected by soil P availability and
881 distribution. New Phytol 225:782-792.
882 Yin X, Struik PC, Romero P, Harbinson J, Evers JB, Van Der Putten PE, Vos JAN
883 (2009) Using combined measurements of gas exchange and chlorophyll
884 fluorescence to estimate parameters of a biochemical C_3 photosynthesis model: a
885 critical appraisal and a new integrated approach applied to leaves in a wheat
886 (*Triticum aestivum*) canopy. Plant Cell Environ 32:448-464.
887 Zait Y, Shtein I, Schwartz A (2019) Long-term acclimation to drought, salinity and
888 temperature in the thermophilic tree *Ziziphus spina*-christi: revealing different
889 tradeoffs between mesophyll and stomatal conductance. Tree Physiol 39:701-716.
890 Zhu XG, Long SP, Ort DR (2010) Improving photosynthetic efficiency for greater
891 yield. Annu Rev Plant Biol 61:235-261.
892

Figure legends

Figure 1 Representative light microscopy images (a, b) and transmission electron microscopy images (c, d) of the leaves of *P. cathayana* females and males grown with NO_3^- or NH_4^+ supply, and with or without salt stress (50 mM NaCl addition for 14 days). Bar = 50 μm for images a and b. Leaf upper epidermis (ue), leaf mesophyll palisade tissue (pl), leaf mesophyll spongy tissue (sp), leaf lower epidermis (le), leaf vascular tissue (v), cell wall (cw), chloroplast (ch) and starch granule (s).

Figure 2 Relationships of the light-saturated rate of photosynthesis with stomatal conductance (g_s) (a) and mesophyll conductance (g_m) (b), and the relationships of g_m with leaf Na^+ concentration (c) and CO_2 drawdown (C_i–C_c) (d) from sub-stomatal cavities (C_i) to chloroplasts (C_c) in *P. cathayana* females (F) and males (M) grown with NO_3^- or NH_4^+ supply, and with or without salt stress. Salt stress application as in Figure 1.

Figure 3 Relationships of CO_2 mesophyll conductance (g_m) with the volume fraction of intercellular air space (f_{ias}) (a), the surface area of mesophyll cells adjacent to intercellular air space (S_m/S) (b), the chloroplast surface area exposed to intercellular air space per leaf area (S_c/S) (c) and the cell wall thickness (T_{cw}) (d) in *P. cathayana* females (F) and males (M) grown with NO_3^- or NH_4^+ supply, and with or without salt stress. Salt stress application as in Figure 1.

915

916 **Figure 4** Quantitative photosynthetic limitations in leaves of *P. cathayana* females (F)
917 and males (M) grown with NO_3^- or NH_4^+ supply, and with or without salt stress. The
918 photosynthetic limitation $dA/A = S_L + MC_L + B_L$. S_L, stomatal limitation; MC_L,
919 mesophyll conductance; B_L, biochemical limitation. Salt stress application as in
920 Figure 1.

921

922 **Figure 5** The share of limitations of g_m among gas-phase (a) and liquid-phase (b)
923 pathways, and absolute values of gas- (c) and liquid-phase (d) conductance in leaves
924 of *P. cathayana* females and males grown with NO_3^- or NH_4^+ supply, and with or
925 without salt stress. Salt stress application as in Figure 1.

926

927 **Figure 6** Anatomical limitations of CO_2 mesophyll conductance (g_m) and CO_2
928 conductance in leaves of *P. cathayana* females (F) and males (M) grown with NO_3^- or
929 NH_4^+ supply with or without salt stress. The share of CO_2 liquid-phase diffusive
930 limitation (a, b) and absolute values of conductance among cytoplasm (g_{cyt1}) and
931 chloroplast stroma (g_{st1}) (c), cell wall (g_{cw}), chloroplast envelope (g_{env}) and plasma
932 membrane (g_{pl}) (d). The g_{st1} variable is the stromal conductance perpendicular to cell
933 walls, and g_{cyt1} is the cytosolic conductance from the plasmalemma inner surface
934 towards the outer surface of chloroplasts. A constant value of 0.0035 m s^{-1} was used
935 for both plasmalemma and chloroplast envelope conductance. Additional components
936 of the diffusion pathway are provided in Figure S2. Salt stress application as in Figure

937 1.

938

939 **Figure 7** Direct and indirect effects of leaf structure, biomass allocation and the
940 surface area of chloroplast exposed to intercellular air spaces per unit leaf area (S_c/S),
941 mesophyll cell area per transverse section width (S/W), CO_2 mesophyll conductance
942 (g_m) and photosynthesis (A) in *P. cathayana* females and males grown with NO_3^- or
943 NH_4^+ supply, and with or without salt stress. Multiple-layer rectangles represent the
944 first component of PCA conducted for the leaf structure and biomass allocation. The
945 arrows indicate the hypothesized direction of causation. The arrow width represents
946 the strength of relationships. Black solid and dotted arrows represent positive and
947 negative relationships, respectively. Grey arrows represent nonsignificant
948 relationships. The leaf structure traits include mesophyll palisade cell area (A_{pl}), the
949 volume fraction of intercellular air space (f_{ias}), leaf thickness (T_l), mesophyll surface
950 area exposed to intercellular air space per unit leaf area (S_m/S), cell wall thickness
951 (T_{cw}), mesophyll length (L_m), mesophyll palisade tissue length (L_{pl}), mesophyll
952 spongy tissue length (L_{sp}), leaf dry mass per unit area (LMA), mesophyll spongy cell
953 density (D_{sp}), chloroplast length (L_{cl}), mesophyll palisade cell density (D_{pl}),
954 chlorophyll content (Chl), chloroplast width (W_{cl}), and mesophyll spongy cell area
955 (A_{sp}). The biomass allocation includes specific root length (SLR), root length density
956 (RLD), stem dry mass (W_s), leaf dry mass (W_l), root dry mass, shoot dry mass/root
957 dry mass (S/R), and leaf dry mass/(stem and root dry mass) (L/(S+R)). The numbers
958 adjacent to the arrows are the standardized path coefficients. The significance values

are shown as follows: ns, not significant; * $0.01< P \leq 0.05$; ** $0.001< P \leq 0.01$; *** $P \leq 0.001$. $X^2 = 7.48$, $p = 0.006$, $RMSE = 0.19$.

Figure 8 A schematic model for leaf anatomical traits, CO_2 diffusion pathway and conductance inside leaves of *P. cathayana* females and males with salt stress under NO_3^- or NH_4^+ supply. The width of the red line represents the strength of CO_2 diffusion conductance into leaves. Blue dots indicate CO_2. g_{cw}, CO_2 transfer conductance through cell wall; g_{env}, CO_2 transfer conductance through chloroplast envelope; g_{pl}, CO_2 transfer conductance through plasma membrane; g_{st1}, the stromal conductance perpendicular to cell wall; g_{st2}, the stromal conductance parallel with the cell wall; g_{cyt1}, CO_2 transfer conductance through cytoplasm from the plasmalemma inner surface to the outer surface of chloroplasts; g_{cyt2}, cytosolic conductance from the plasmalemma inner surface to the outer surface of chloroplasts; T_{leaf}, leaf thickness; P, mesophyll palisade tissue; S, mesophyll spongy tissue; C, chloroplast. Salt stress application as in Figure 1. The relative values of the liquid-phase components based on the Figure 6 and Figure S2. Values of g_{cyt2} and g_{cyt1} under NO_3^- supply, andg_{st1}, g_{cyt1}, g_{cyt2} and g_{cw} under NH_4^+ supply were lower in females than in males. The values of g_{st2} under NO_3^- supply were higher in females than females.

981

982 **Figure 1**

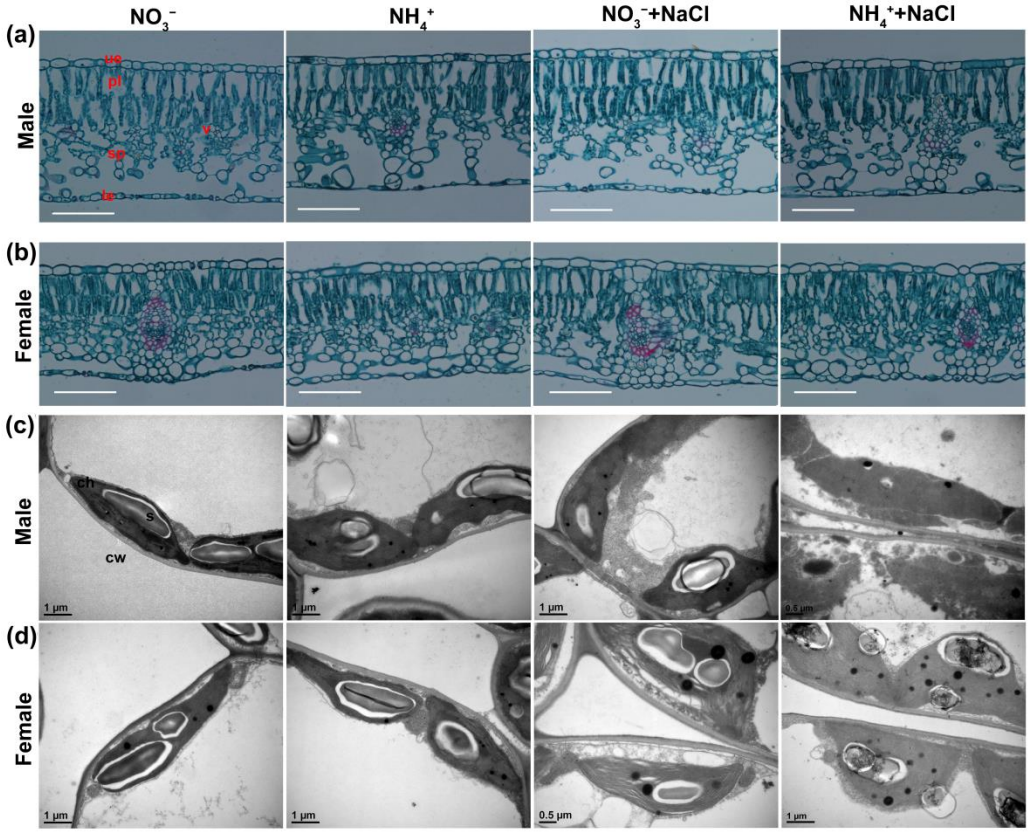

983

984

985

986

987

988

989

990

991

992

993

Figure 2

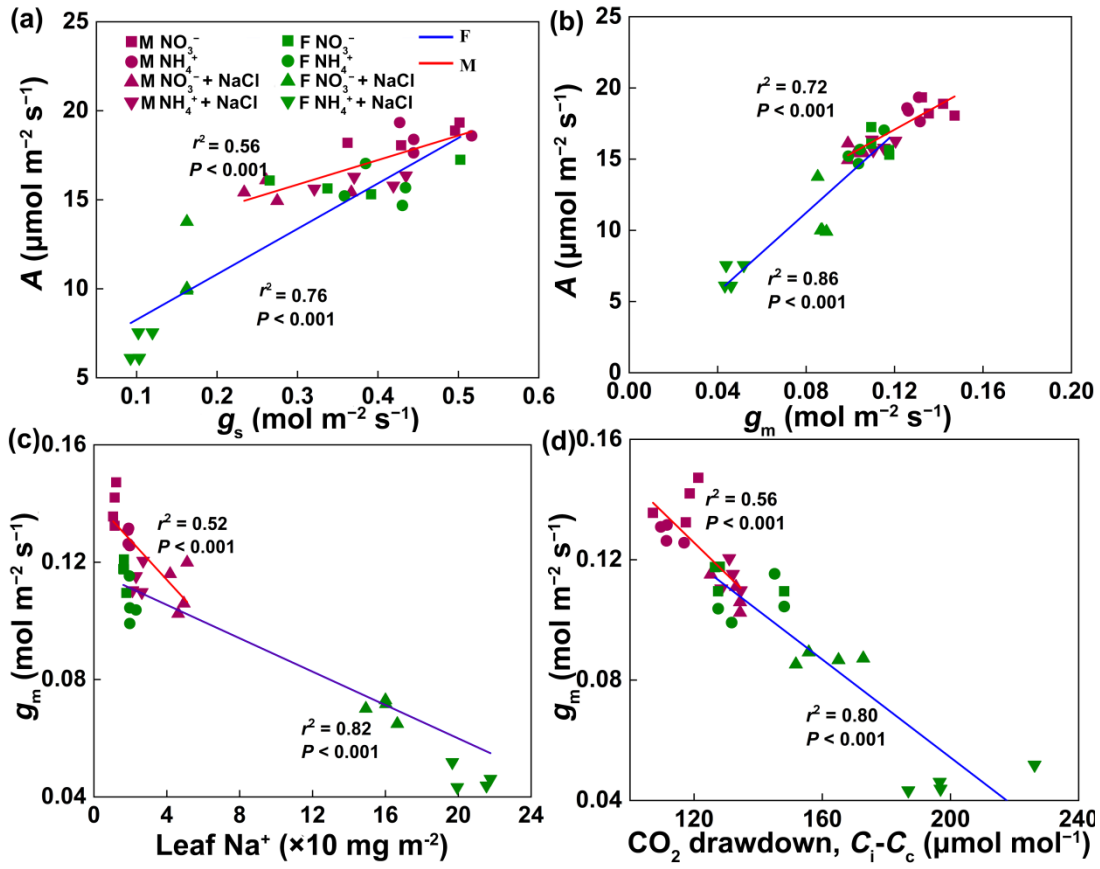
(a)
M NO_3^-
M NH_4^+
M NO_3^- + NaCl
M NH_4^+ + NaCl
F NO_3^-
F NH_4^+
F NO_3^- + NaCl
F NH_4^+ + NaCl
F
M
r^2 = 0.56
P < 0.001
r^2 = 0.76
P < 0.001
A (μmol m^{-2} s^{-1})
g_s (mol m^{-2} s^{-1})
(b)
r^2 = 0.72
P < 0.001
r^2 = 0.86
P < 0.001
A (μmol m^{-2} s^{-1})
g_m (mol m^{-2} s^{-1})
(c)
r^2 = 0.52
P < 0.001
r^2 = 0.82
P < 0.001
g_m (mol m^{-2} s^{-1})
Leaf Na^+ (×10 mg m^{-2})
(d)
r^2 = 0.56
P < 0.001
r^2 = 0.80
P < 0.001
g_m (mol m^{-2} s^{-1})
CO_2 drawdown, C_i-C_c (μmol mol^{-1})

Figure 3

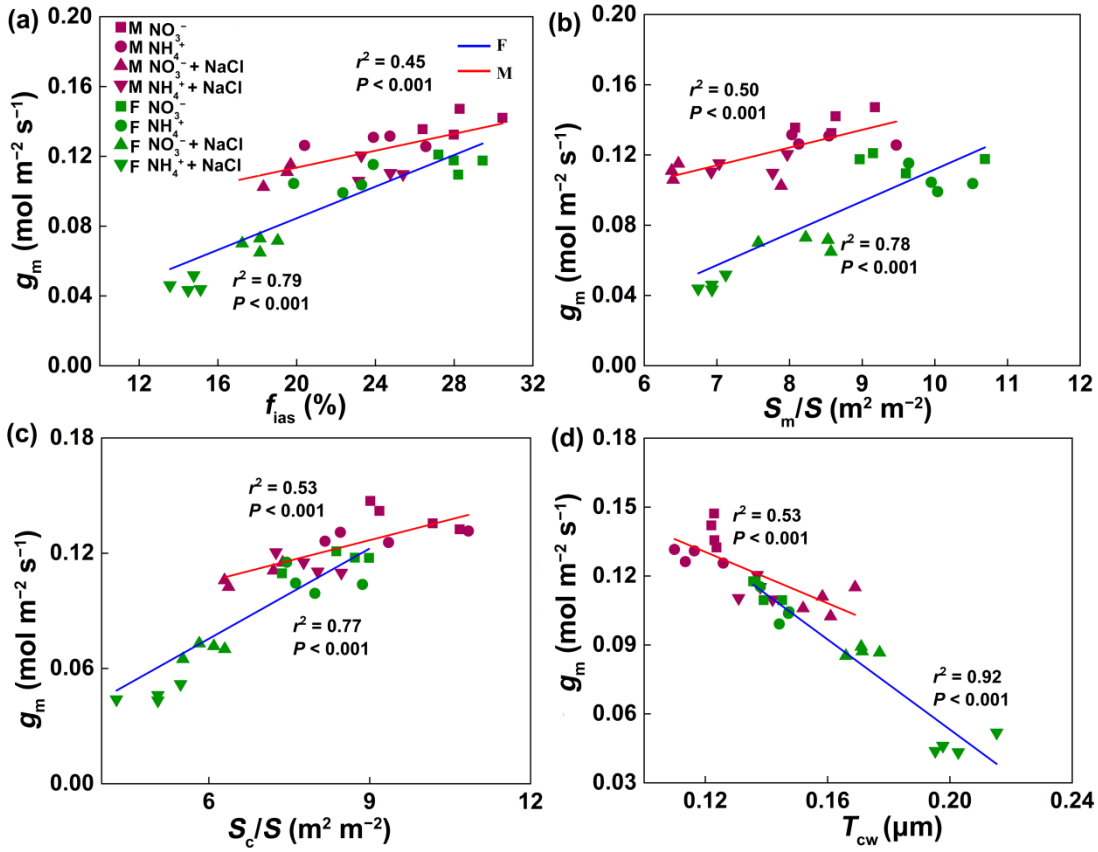
(a)
M NO_3^-
M NH_4^+
M NO_3^- + NaCl
M NH_4^+ + NaCl
F NO_3^-
F NH_4^+
F NO_3^- + NaCl
F NH_4^+ + NaCl
F
M
r^2 = 0.45
P < 0.001
r^2 = 0.79
P < 0.001
g_m (mol m^{-2} s^{-1})
f_{ias} (%)
(b)
r^2 = 0.50
P < 0.001
r^2 = 0.78
P < 0.001
S_m/S (m^2 m^{-2})
(c)
r^2 = 0.53
P < 0.001
r^2 = 0.77
P < 0.001
S_c/S (m^2 m^{-2})
(d)
r^2 = 0.53
P < 0.001
r^2 = 0.92
P < 0.001
T_{cw} (μm)

Figure 4

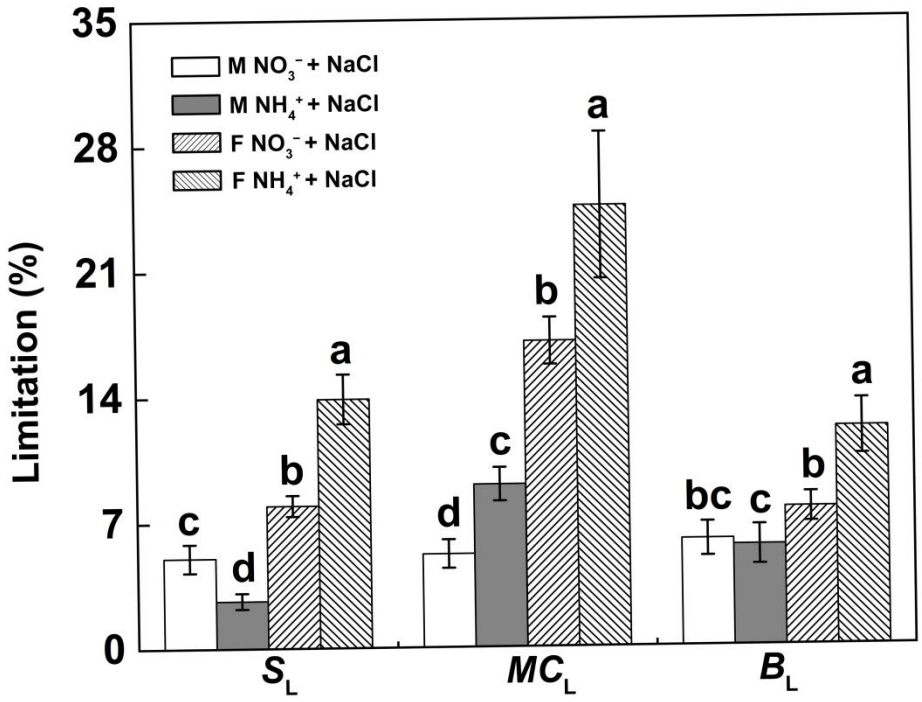
35
28
21
14
7
0
Limitation (%)
M NO3− + NaCl
M NH4+ + NaCl
F NO3− + NaCl
F NH4+ + NaCl
c
d
b
a
d
c
b
a
bc
c
b
a
SL
MCL
BL

1034

1035 **Figure 5**

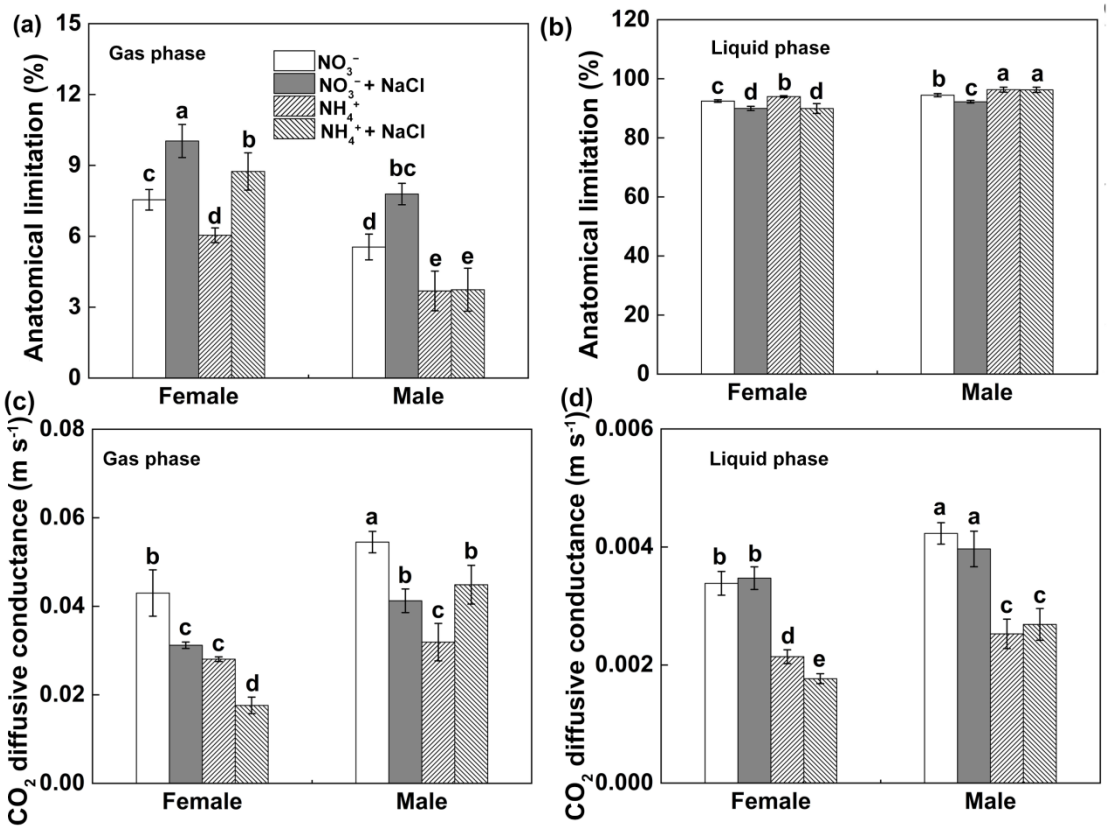

1036

Figure 6

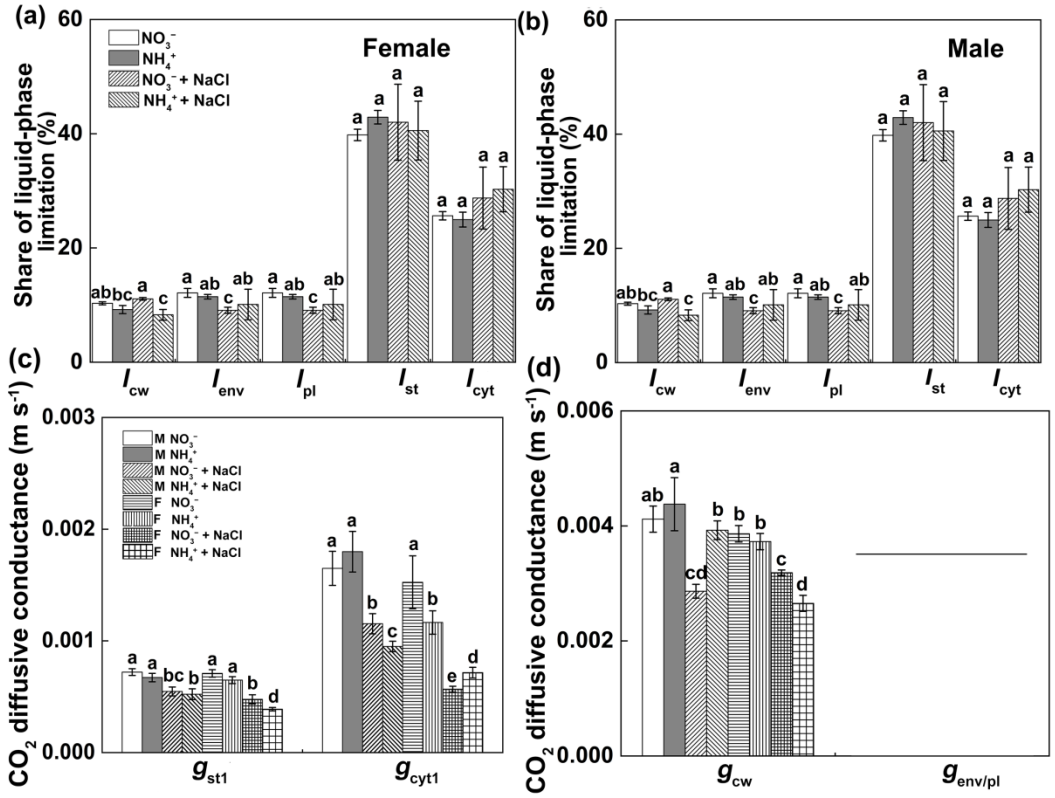
(a)
Female
(b)
Male
Share of liquid-phase limitation (%)
NO_3^-
NH_4^+
NO_3^- + NaCl
NH_4^+ + NaCl
l_{cw}
l_{env}
l_{pl}
l_{st}
l_{cyt}
(c)
(d)
CO_2 diffusive conductance (m s^{-1})
M NO_3^-
M NH_4^+
M NO_3^- + NaCl
M NH_4^+ + NaCl
F NO_3^-
F NH_4^+
F NO_3^- + NaCl
F NH_4^+ + NaCl
g_{st1}
g_{cyt1}
g_{cw}
$g_{env/pl}$

Figure 7

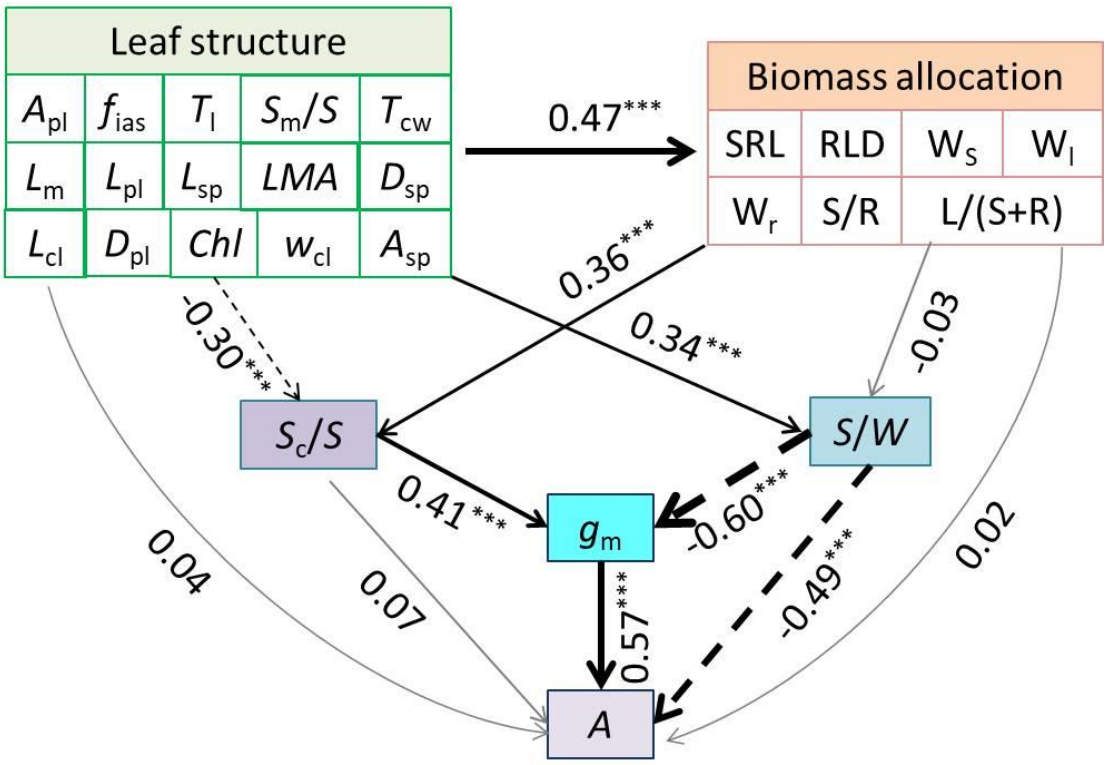
Leaf structure
A_{pl} f_{ias} T_l S_m/S T_{cw}
L_m L_{pl} L_{sp} LMA D_{sp}
L_{cl} D_{pl} Chl w_{cl} A_{sp}
Biomass allocation
SRL RLD W_S W_l
W_r S/R L/(S+R)
0.47***
0.36***
0.34***
-0.30***
-0.03
S_c/S
S/W
0.41***
g_m
-0.60***
-0.49***
0.57***
0.04
0.07
0.02
A

1064 **Figure 8**

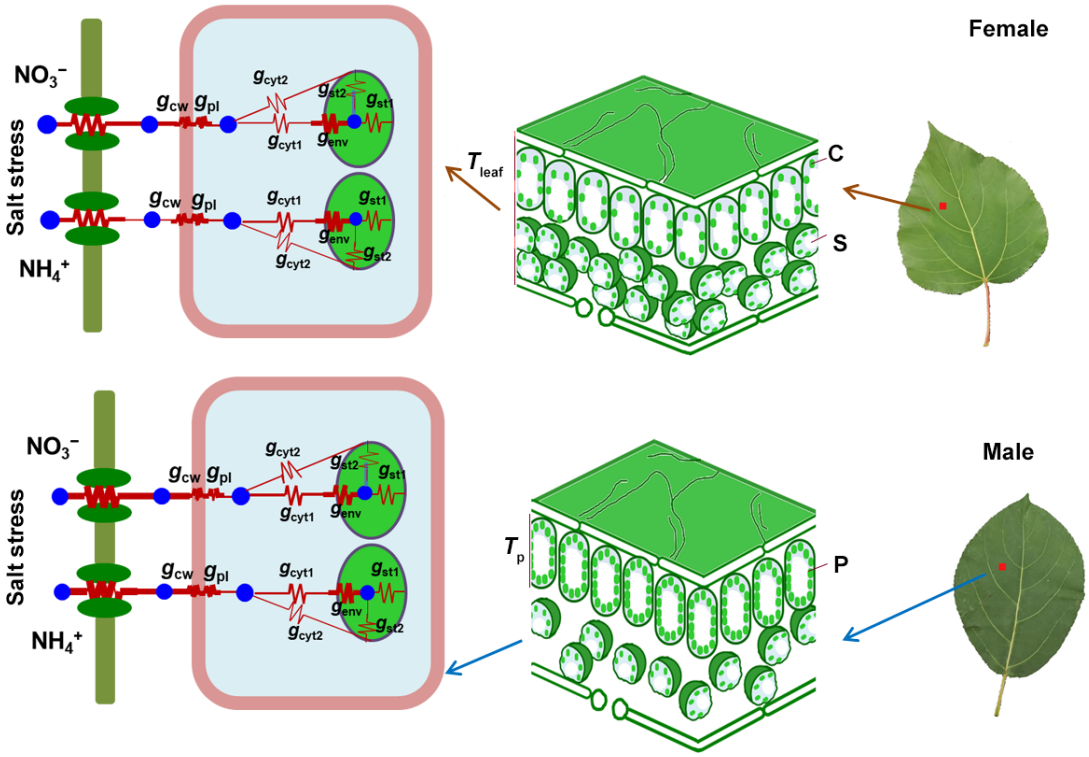

1065

Table 1 Leaf biomass and area, leaf structural and gas exchange characteristics, leaf construction cost and root traits in *P. cathayana* females and males under NO_3^- or NH_4^+ supply, and with or without salt stress.

Salt	N form	Sex	Leaf biomass	Leaf area	*LMA*	Leaf CC	F_v/F_m	*J*	V_{cmax}	SRL	RLD	Root biomass
0	NO_3^-	Female	14.14±0.93a	85.14±5.90a	37.83±3.57d	1.39±0.01a	0.814±0.01a	47.45±3.86a	65.99±1.68b	6.91±0.50cd	1.70±0.15a	8.04±0.44a
0	NO_3^-	Male	8.69±0.28cd	51.65±6.57d	45.20±2.18c	1.39±0.01a	0.808±0.01a	50.95±2.72a	74.44±4.43a	7.27±1.08cd	0.671±0.06e	4.08±0.35d
0	NH_4^+	Female	12.83±1.46b	72.09±5.54b	36.62±2.78d	1.37±0.06ab	0.815±0.01a	35.18±3.85b	58.18±5.12c	8.25±0.78c	1.24±0.13b	6.87±0.44b
0	NH_4^+	Male	8.41±0.74cd	43.77±1.20d	45.54±1.10c	1.39±0.01a	0.794±0.01b	47.78±0.99a	66.17±3.44b	6.87±1.41cd	0.847±0.06d	5.38±0.25c
50	NO_3^-	Female	9.54±0.45c	68.28±4.15bc	51.67±3.09b	1.37±0.004ab	0.769±0.01cd	17.93±2.81d	51.47±4.09d	13.611.15a	1.29±0.05b	7.12±0.56b
50	NO_3^-	Male	8.06±0.60de	50.60±5.96d	54.58±2.44ab	1.39±0.01a	0.773±0.01c	35.13±3.90b	65.79±3.12b	6.51±0.67d	1.56±0.10a	4.54±0.28d
50	NH_4^+	Female	8.44±0.95cde	63.10±4.61c	58.33±4.46a	1.35±0.06c	0.757±0.01d	13.88±1.59d	42.10±2.53e	10.75±1.09b	0.784±0.06de	4.57±0.31d
50	NH_4^+	Male	6.64±1.02f	45.93±2.18d	53.06±2.40b	1.41±0.01a	0.790±0.01b	24.18±2.16c	58.68±2.64c	7.39±0.92cd	1.01±0.14c	3.25±0.40e
		P_{se}	***	***	**	***	ns	***	***	***	***	***
		P_{sa}	***	***	***	ns	***	***	***	***	ns	***
		P_n	***	***	ns	ns	ns	***	***	ns	***	***
		$P_{se\times sa}$	***	*	***	***	***	**	**	***	***	**
		$P_{se\times n}$	Ns	ns	ns	***	ns	ns	ns	ns	***	***
		$P_{sa\times n}$	Ns	**	Ns	ns	ns	ns	ns	*	***	***
		$P_{se\times sa\times n}$	Ns	ns	*	ns	**	***	ns	***	***	*

Leaf biomass (g); leaf area (cm^2); *LMA* ($g\ m^{-2}$), leaf dry mass per unit leaf area; leaf CC ($g\ glucose\ g^{-1}$), leaf construction cost; F_v/F_m, maximum quantum efficiency of PSII photochemistry; *J* ($\mu mol\ m^{-2}\ s^{-1}$), photosynthetic electron transport rate from chlorophyll fluorescence (Eq. 2); V_{cmax} ($\mu mol\ m^{-2}\ s^{-1}$), the maximum carboxylase activity of Rubisco; SRL ($m\ g^{-1}$), specific root length; RLD ($cm\ cm^{-3}$), root length density; root biomass (g). P_{se}, sex effect; P_{sa}, salt effect; P_n, N form effect (NO_3^- and NH_4^+); $P_{se\times sa}$, the interaction effect of sex and salt stress; $P_{n\times sa}$, the interaction effect of N forms and salt stress; $P_{se\times n}$, the interaction effect of sex and N forms; $P_{se\times n\times sa}$, the interaction effect of sex, N forms and salt stress. Different letters indicate significant differences between treatments ($P<0.05$, three-way ANOVA followed by Duncan's tests). Data are mean ± SE ($n = 4$). The significance values are shown as follows: ns, not significant; * $0.01< P \leq 0.05$; ** $0.001< P \leq 0.01$; *** $P \leq 0.001$.

Table 2 Leaf thickness and anatomical traits in *P. cathayana* females and males grown under NO_3^- or NH_4^+ supply, and with or without salt stress. Data are mean ± SE (n = 4).

Salt	N form	Sex	f_{ias} (%)	S_m/S	S_c/S	S/W	T_l	T_{cw}	D_{chl}	L_{chl}	T_{chl}	$\Delta L_{cyt,1}$	ΔL_{cyt2}
0	NO_3^-	Female	28.21±0.93a	9.60±0.77ab	7.36±0.99bc	71.5±6.0b	171.3±3.2b	0.139±0.004d	12.8±0.9cd	5.9±0.6ab	1.7±0.09c	0.106±0.13e	0.864±0.040e
0	NO_3^-	Male	28.28±1.67a	7.76±0.22c	7.01±0.24c	35.6±4.7d	220.6±17.8a	0.123±0.001e	16.3±1.0a	6.1±0.6a	1.3±0.06e	0.093±0.002e	0.821±0.004e
0	NH_4^+	Female	22.35±1.78b	10.04±0.36a	7.98±0.63ab	72.9±0.91b	177.8±8.8b	0.144±0.004d	11.5±0.6d	4.7±0.6c	1.7±0.06c	0.138±0.10d	0.969±0.025d
0	NH_4^+	Male	23.90±2.58b	8.54±0.66bc	8.45±0.65bc	42.5±5.7d	216.1±44.2a	0.116±0.007e	13.8±1.0bc	6.2±0.5a	1.6±0.09cd	0.074±0.003f	0.877±0.034e
50	NO_3^-	Female	18.14±0.74c	6.93±0.46d	5.93±0.69d	82.7±1.5a	177.3±1.9b	0.171±0.004b	8.8±1.0e	5.2±0.6bc	2.6±0.2b	0.202±0.016b	1.38±0.042b
50	NO_3^-	Male	22.90±2.62b	8.40±1.09bc	6.31±0.75c	52.5±8.9c	212.3±2.7a	0.160±0.007c	16.3±1.3a	5.9±0.2ab	1.4±0.05de	0.162±0.016c	1.02±0.058d
50	NH_4^+	Female	14.49±0.67d	6.22±0.16d	4.96±0.63e	89.2±2.6a	177.6±3.9b	0.203±0.009a	9.0±0.8e	5.2±0.5bc	3.2±0.3a	0.279±0.018a	1.59±0.11a
50	NH_4^+	Male	23.29±2.55b	8.97±1.45abc	7.13±0.68c	41.0±4.4d	212.5±9.2a	0.137±0.005d	14.5±0.6b	6.3±0.5a	1.6±0.1cd	0.218±0.007b	1.22±0.078c
		P_{se}	***	ns	***	***	***	***	***	***	***	***	***
		P_{sa}	***	***	***	***	ns	***	***	ns	***	***	***
		P_n	***	ns	ns	ns	ns	ns	***	ns	***	***	***
		$P_{se\times sa}$	***	***	ns	ns	ns	***	***	ns	***	ns	***
		$P_{se\times n}$	***	ns	ns	*	ns	***	*	*	ns	***	ns
		$P_{sa\times n}$	***	ns	ns	*	ns	ns	ns	ns	*	***	**
		$P_{se\times sa\times n}$	Ns	ns	*	***	ns	***	ns	ns	**	ns	ns

1086 f_{ias} (%), the volume fraction of intercellular air space per unit leaf area; S_m/S (m^2 m^{-2}), mesophyll surface area exposed to intercellular air space
1087 per unit leaf area; S_c/S (m^2 m^{-2}), chloroplast surface area exposed to intercellular air space per unit leaf area; S/W (μm^2 μm^{-1}), mesophyll cell
1088 area per transverse section width; T_l (μm), leaf thickness; T_{cw} (μm), cell wall thickness; D_{chl} (no. no), chloroplast density; L_{chl} (μm), chloroplast
1089 length; T_{chl} (μm), chloroplast thickness; $\Delta L_{cyt,1}$ (μm), the vertical distance between the chloroplasts and cell walls; ΔL_{cyt2} (μm), the distance
1090 between the neighboring chloroplasts. P_{se}, sex effect; P_{sa}, salt effect; P_n, N form effect (NO_3^- and NH_4^+); $P_{se\times sa}$, the interaction effect of sex and
1091 salt stress; $P_{n\times sa}$, the interaction effect of N forms and salt stress; $P_{se\times n}$, the interaction effect of sex and N forms; $P_{se\times n\times sa}$, the interaction effect of
1092 sex, N forms and salt stress. Different letters indicate significant differences between treatments ($P<0.05$, three-way ANOVA followed by
1093 Duncan's tests). Data are mean ± SE (n = 4). The significance values are shown as follows: ns, not significant; * $0.01< P \leq 0.05$; ** $0.001< P \leq$
1094 0.01; *** $P \leq 0.001$.